Structural properties of PbTe/CdTe interfaces from first principles

R. Leitsmann,* L. E. Ramos, and F. Bechstedt
Institut für Festkörpertheorie und -optik, Friedrich-Schiller-Universität Jena, Max-Wien-Platz 1, 07743 Jena, Germany
(Received 24 May 2006; published 17 August 2006)

The structural and energetic properties of the PbTe/CdTe(100), (110), and (111) interfaces are investigated using an *ab initio* pseudopotential method within a slab approximation. A scheme is proposed to calculate interface energies for polar faces with a resulting dipole moment. The atomic relaxation gives rise to similar effects as those observed for free surfaces. At (110) interfaces the rebonding leads to pronounced additional lateral displacements. The PbTe/CdTe(111) interface is the most energetically stable interface studied. The interface energies are used to predict the equilibrium crystal shape of a PbTe quantum dot embedded in a CdTe host matrix by means of a Wulff construction.

DOI: 10.1103/PhysRevB.74.085309 PACS number(s): 68.35.Ct, 68.35.Md, 68.37.Lp, 68.65.Hb

I. INTRODUCTION

Fabrication of electronic, optoelectronic, and sensoric devices has renewed the interest in self-organization and self-assembly of nano-objects (dots, wires, molecules) in solid matrices as well as on solid surfaces and interfaces. A variety of structures and materials is found to be promising for future applications in optoelectronics or nanoelectronics. Nanostructures such as quantum dots (QDs) with quantum confinement of the electron or the hole wave functions are of particular interest, since they exhibit properties similar to those of atoms[1,2] or molecules.[2,3] Heiss and co-workers[4] recently demonstrated that PbTe QDs in a CdTe host matrix exhibit an intense room-temperature mid-infrared luminescence. The availability of light sources in the mid-infrared spectral region is crucial for many applications, e.g., molecular spectroscopy and gas-sensor systems for environmental monitoring or medical diagnostics. High-resolution transmission electron microscopy (HRTEM) studies[4,5] demonstrate for the annealed PbTe/CdTe systems the existence of rather ideal PbTe nanocrystals with (111), (100), and (110) interfaces with the CdTe host matrix. Their diameters vary in the range of 2 to 10 nm. There is seemingly an almost lack of imperfections related to other QDs prepared within a Stranski-Krastanov growth process, such as an interconnecting two-dimensional wetting layer, inhomogeneous alloying with the host material, or shape asymmetries.[6] The preceding annealing procedure and the almost vanishing lattice mismatch between PbTe and CdTe suggest a situation for the nanostructured system close to thermal equilibrium. Consequently, the shape of such embedded PbTe QDs should be mainly determined by the interface energetics and hence the PbTe/CdTe interface energies.

The determination of interface energies needs the knowledge about the atomic structure. Unfortunately, practically nothing is known in the case of the PbTe/CdTe interfaces. To the best of our knowledge, properties of such interfaces were studied only in growth experiments and by few authors.[7–10] There are practically no theoretical predictions for PbTe/CdTe heterostructures. However, there are experimental and theoretical studies of the clean surfaces, in particular for CdTe (see Refs. 11–13 and references therein). For the PbTe(001) surface both experimental[14] and total-energy[15] investigations indicate a remarkable rumpling effect.[16] For the nonpolar (001) surface of the PbTe rocksalt crystal, each atomic layer contains the same number of cations and anions with the same bulk z coordinate in such a xy plane. In the presence of a surface the equilibrium atomic positions are not fixed by symmetry and, hence, can be different for different atomic species, inducing a surface rumpling.

The theoretical investigation of the tellurides PbTe and CdTe, in particular of their surfaces and interfaces, is a challenging task for different reasons. There is a remarkable ionic contribution to the chemical bonding in PbTe and CdTe. The ionicity coefficients f_i in the Phillips scale are 0.67 and 0.65 for CdTe and PbTe, repectively.[17,18] Theoretical studies of PbTe make an estimate of about 1.5 electrons for the charge transfer from Pb to Te, demonstrating the strong ionic character of this material.[19] CdTe has a nonvanishing charge distribution along the Cd-Te bonds suggesting a covalent contribution to its bonds.[20] As a consequence PbTe crystallizes in the rocksalt (RS) structure with the space group $Fm3m$ (O_h^5), whereas the more covalent CdTe crystallizes in the zinc-blende (ZB) structure with space group $F\bar{4}3m$ (T_d^2). Although both crystal structures have a fcc Bravais lattice, their ideal surface geometries are different.[16] For instance, while for rocksalt the (001) surface is nonpolar and hence represents the cleavage face of the crystal, the [001] orientation in the ZB structure leads to a polar (cation-or anion-terminated) surface. In the ZB case the only nonpolar cleavage face is (110). The different atomic arrangements at surfaces of the same orientation, but of bulk with different crystal structures, result in a drastic misfit of the dangling bonds at the interface with respect to position, orientation, and hybridization degree.

PbTe and CdTe contain heavy elements and this fact leads to relatively long bond lengths and narrow fundamental energy gaps. Another difficulty related to tellurides is the strong relativistic effects.[13,21–23] A spin-orbit splitting of about 1 eV is measured for the uppermost valence bands at an L point (PbTe) (Ref. 23) or at the Γ point (CdTe).[24,25]

The determination of surface and interface energies is a difficult task for both experimental and theoretical investigations, since they depend on the surface and interface orientations.[16] So far, for a variety of orientations, only interface energies for group-IV crystals surrounded by vacuum

 ©2006 The American Physical Society

were calculated (see Ref. 26 and references therein). While the measurements of interface energies are difficult, theoretical estimates of those quantities require very time-consuming computer calculations to determine the interface atomic structure and energy values, which correspond to an isolated interface or surface.

The usual approximation to describe interfaces between two different materials or even different crystal structures is the repeated-slab (or superlattice) approximation[16,27–30] independent of their orientation and lattice mismatch. Two thin films are combined to a unit cell along the normal direction. The advantage of the slab approximation is the conservation of a three-dimensional translational symmetry, whereas its disadvantage is the need of the simultaneous treatment of two interfaces. Only in the cases of electrostatically neutral atomic layers perpendicular to the interface normal, e.g., (110) of zinc blende and (100) as well as (110) of rocksalt, and the same bonding geometry one can construct a symmetric slab with identical interfaces. Slabs mimicking polar surfaces, e.g., (001) and (111) of zinc blende and (111) of rocksalt, display a net charge in each layer and on the two surfaces themselves. The combination of two polar slabs or of a polar slab with a nonpolar one leads to a supercell with chemically, structurally, and electrostatically different interfaces, which are indicated in the following by *A* (cation terminated) and *B* (anion terminated). The two different polarities of the two interfaces will introduce a spurious electric field in both material slabs of the supercell, which may affect the interface geometry and other results.

In the case of polar surfaces, i.e., of slabs with *A* and *B* surfaces separated by vacuum, a slab dipole potential is created. This effect can be partially corrected using the so-called dipole correction suggested by Neugebauer and Scheffler,[31,32] where a potential step is introduced in the vacuum region. For interfaces, an accurate and efficient treatment is still an open question. This holds particularly for the interfaces between the strong ionic materials PbTe and CdTe with different crystal structures.

The three-dimensional equilibrium shape of a small crystal at a certain temperature can be obtained from the anisotropy of the surface free energy in the thermodynamic limit.[16] In a Wulff construction[33,34] one neglects kinetic and strain effects and the influence of edge and vertex energies. Such a construction should also be possible for nanocrystals embedded in a solid matrix, at least in the thermodynamic equilibrium, as discussed above for the RS-PbTe nanocrystals in a crystalline ZB-CdTe layer. This however requires knowledge of the corresponding interface energies for the most important orientations.

In this paper, we investigate the PbTe/CdTe (110), (100) and (111) interfaces. In Sec. II, we describe the method applied to calculate the total energies as well as a method to calculate interface energies within the slab approximation in an accurate and efficient way. The results for the interface geometries and energies are presented and discussed in Sec. III. The actual three-dimensional shape of the PbTe nanocrystallites is then obtained from the free interface energies using the Wulff construction. A summary of the results and conclusions is given in Sec. IV.

TABLE I. Equilibrium lattice constants a_0 (in Å) and bulk moduli B (in GPa) of PbTe and CdTe crystals. LSDA indicates the local-spin-density approximation.

		LDA	LSDA	Experiment
PbTe	a_0	6.385	6.374	6.443[a]
	B	48.9	46.6	40[a]
CdTe	a_0	6.421	6.423	6.48[b]
	B	46.6	45.6	42[c]

[a]Reference 21.
[b]Reference 39.
[c]Reference 46.

II. MODELING OF INTERFACES

A. Total-energy calculation method

We applied density-functional theory (DFT) within local-density approximation (LDA) as implemented in the Vienna *ab initio* simulation package (VASP).[35,36] To evaluate the influence of relativistic effects we performed test calculations including noncollinear spins;[37] in particular the spin-orbit coupling was taken into account. The interaction of the valence electrons with the remaining ions is modeled by pseudopotentials generated within the projector augmented wave method.[38] In II-VI semiconductors the outermost *d* states give rise to shallow semicore bands, which contribute essentially to the chemical bonding.[39] Therefore, we treat the outermost Cd and Pb *d* electrons as valence electrons. An energy cutoff of 15 Ry for the plane-wave basis is sufficient to obtain converged structural properties. The total-energy expression contains a Brillouin zone integration, which is replaced by a summation over special points of the Monkhorst-Pack type.[40] For the bulk fcc structures we apply $11\times11\times11$ **k**-point meshes, whereas for the repeated-slab systems, we use $5\times7\times1$, $7\times7\times1$, and $9\times5\times1$ **k**-point meshes for the (110), (100), and (111) interfaces, respectively. The atomic geometries are allowed to relax until the Hellmann-Feynman forces are smaller than 20 meV/Å.

B. Slab approximation

In order to model the different PbTe/CdTe interfaces we use the common slab approximation,[27] and take advantage of two facts. First of all the two cubic crystals CdTe and PbTe have nearly the same lattice constants a_0 and isothermal bulk moduli B (see Table I). The lattice mismatch is smaller than 1%. This enables us to construct rather strain-free slabs. In all calculations we use an averaged (theoretical) lattice constant of a_0=6.41 Å, which is closer to the equilibrium lattice constant of bulk CdTe. Since PbTe quantum dots are embedded in a CdTe matrix, it is a reasonable assumption that the PbTe lattice tends to follow the lattice constant of the CdTe host matrix. Secondly the two crystals have different structures, rocksalt and zinc blende, but the cation and anion sublattices have the same fcc translational symmetry as the common Bravais lattice. The two sublattices are only differently displaced with respect to each other by one-quarter (ZB) or one-half (RS) of a body diagonal. Without lack of generality

we start the interface modeling with a common fcc Te sublattice in the entire supercell system. For the construction of the unrelaxed ideal slab geometries in the supercells, we complete the PbTe slab by a fcc Pb sublattice displaced by $(\frac{1}{2},\frac{1}{2},\frac{1}{2})a_0$, whereas in the CdTe slab of the supercell the fcc Cd sublattice is displaced by $(\frac{1}{4},\frac{1}{4},\frac{1}{4})a_0$.

Slabs with an *AB* stacking and one common sublattice give rise to different interface separations at interfaces with different terminations. To check the validity of the construction scheme, we compared the results of (100) interface slabs with a common Te sublattice with a (100) slab system of equal interface separations but a small offset between the Te sublattices in each of the slabs of the supercell. We found that the total free energy of the slab system with fixed Te sublattice is the smallest. From this fact it can be understood that the slabs with equal interface separation are energetically less stable than the slabs used in our calculations.

One major challenge of the slab approximation is the treatment of polar interfaces, which in the ZB or RS case are the interfaces with [100] and [111] orientations. The superior electric field, introduced by periodic boundary conditions, results in an artificial electrostatic potential Φ. The difference of its plane average $\Delta\Phi$ (see Fig. 2 below) between the left- and right-hand sides of a material slab can be calculated by

$$\Delta\Phi = -\frac{\sigma}{\epsilon_0\tilde{\epsilon}^2}\frac{d_1 d_2}{d_1+d_2}, \tag{1}$$

where d_1 and d_2 are the thicknesses of material slabs 1 and 2, respectively. We have introduced the average dielectric constant

$$\tilde{\epsilon} = \frac{\epsilon^2_{zz} d_1 + \epsilon^1_{zz} d_2}{d_1+d_2}, \tag{2}$$

where ϵ^1_{zz} and ϵ^2_{zz} are the zz components of the dielectric tensor of materials 1 and 2, and ϵ_0 denotes the permittivity of the vacuum.

The induced interface charge density σ is defined by the difference of the zero-field polarization fields P_1 and P_2 in the materials 1 and 2,

$$\sigma = \frac{P_1 - P_2}{\tilde{\epsilon}}. \tag{3}$$

Since the zero-field polarization is proportional to the interface dipole density μ divided by the material thickness,

$$P_i \sim \frac{\mu}{d_i}, \tag{4}$$

which is true in the case of cubic materials, $\Delta\Phi$ is independent of the slab size. In other words if one increases the slab, the slope of the artificial dipole potential and thus the resulting nonphysical forces decrease. Therefore we have to construct large-sized supercells to achieve convergence with respect to the atomic displacements at the interface. Each slab of such an electrostatically neutral and stoichiometric supercell should be a multiple of the *irreducible crystal slab* for a given orientation,[16] in order to guarantee translational invariance along the interface normals. These irreducible crystal slabs consist of six atomic layers (three bilayers of cations and anions) for ZB and RS (111), four atomic layers (two bilayers) for ZB (100), and two neutral atomic layers for ZB and RS (110) and RS (100). Together with the condition of equal numbers of Cd and Pb atoms in each supercell, we use 28-(bi)layer slabs for the [110] and [100] orientations and a 24-(bi)layer slab for the [111] orientation. Further enlargement of the slabs would change the resulting interface displacements by less then 0.05 Å. Tests gave no evidence for an interface reconstruction such as 2×1 (which we widely studied) for all considered orientations. So simple 1×1 interface cells are used. Because of the equivalence of the two sublattices in rocksalt and zinc blende, fortunately, lateral unit cells of the same size and shape can be constructed. A general construction of CdTe/PbTe supercells consisting of two crystal slabs, as shown in Fig. 1 for the case of a (110) interface.

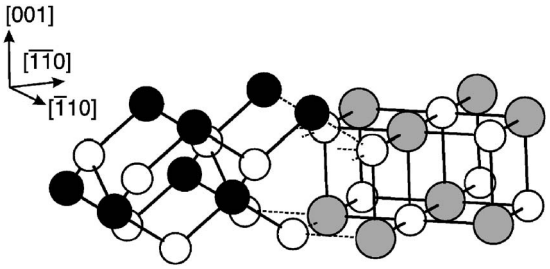

FIG. 1. Schematic representation of a (110) supercell consisting of CdTe and PbTe slabs. The Te (Cd, Pb) atoms are presented by open (filled, shaded) circles. Note the coordination incompatibility across the interface plane (dashed lines).

C. Interface energies

The interface energies or more exactly the excess free interface energies $E^{\text{inter}}_{\text{free}}(hkl)$ can be calculated in the low-temperature limit from the difference of the total energy of the supercell $E^{\text{tot}}[\text{CdTe/PbTe}](hkl)$ and the corresponding total energies of slabs with bulk atomic structures $E^{\text{tot}}[\text{CdTe}](hkl)$ and $E^{\text{tot}}[\text{PbTe}](hkl)$ as

$$E^{\text{inter}}_{\text{free}}(hkl) = \frac{1}{2}\Big[E^{\text{tot}}[\text{CdTe/PbTe}](hkl) - \frac{1}{2}E^{\text{tot}}[\text{CdTe}](hkl) - \frac{1}{2}E^{\text{tot}}[\text{PbTe}](hkl)\Big]. \tag{5}$$

A drawback of the supercell method is that one can only calculate the average value of the two intrinsically formed interfaces. For crystal orientations that lead to nonpolar interfaces, it is always possible to construct slabs with identical interfaces, whereas for crystal orientations that lead to polar interfaces that is not possible. Therefore, when we discuss interface energies of polar slabs, we refer always to the average energy value of the two different *A* and *B* interfaces. There exists a consistent method to calculate surface and interface energies of isolated lateral objects. It is based on the energy-density formalism of Chetty and Martin[41] and can

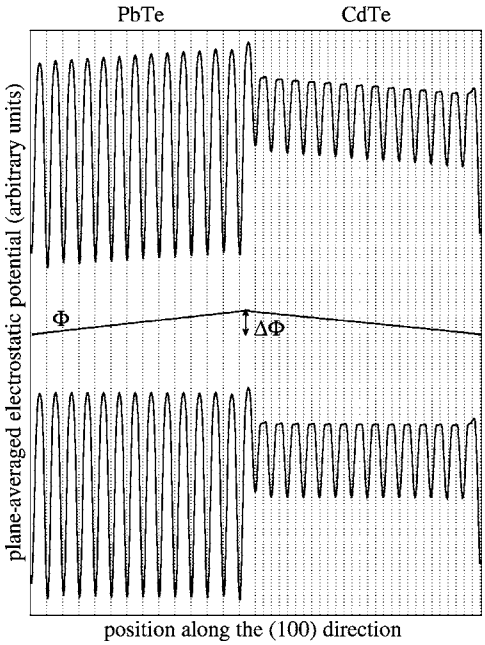

FIG. 2. Plane-averaged electrostatic potential along the [100] direction of a (100) interface supercell (top panel), the artificial potential Φ (middle panel), and the resulting electrostatic potential with compensation (bottom panel). The vertical dotted lines mark the ideal atomic positions.

be combined with a structural relaxation, though in this case it demands too much computer time.[42] For free surfaces whose stoichiometry and geometry are allowed to vary with respect to the bulk atomic positions, the variation of the surface energy with the polarity is not too strong. In the case of ZB-InAs the surface energy per area varies between 42 meV/Å^2 [for $A(111)$] and 49 meV/Å^2 [for $B(111)$].[43] In our case the small variations of the energies can be neglected, since the interfaces are stoichiometric and their energies are, therefore, independent of the chemical potential of the constituents.

For the Wulff construction we apply interface energies that arise from different slab calculations. To minimize numerical uncertainties due to the different supercells we use the same slab sizes, the same MP **k**-point sets, and the same energy cutoff in the calculations for all three interfaces. We make an estimate of about 0.01 J/m^2 for the error bar of the nonpolar interface energies due to numerical uncertainties. In the case of polar slabs the artificial electrostatic potential Φ (see Fig. 2) causes an additional contribution to the total energy. We follow the suggestions by Neugebauer and Scheffler,[31] who introduced a dipole field that compensates the artificial interaction of A and B surfaces across the vacuum region. To avoid the resulting potential jump, we have generalized this procedure developed for the solid-adlayer-vacuum interfaces to solid-solid interfaces, and have introduced a dipole correction that compensates the artificial field within the periodic supercell calculations. It consists of two parts, a compensating potential that cancels the artificial electric field and an energy correction term. According to a remark in Ref. 44 the complete expression for the energy correction is

$$E_{\mathrm{dipc}} = \frac{1}{2}\left(\int \Phi(\mathbf{r}) n(\mathbf{r}) d^3 r - \sum_I Z_I \Phi(\mathbf{R}_I) \right), \tag{6}$$

where Z_I is the valency, $\mathbf{R}_I$ is the position of the Ith ion, and $n(\mathbf{r})$ is the valence electron density. To calculate the interface energies of polar slabs with the same accuracy as for nonpolar ones, we use the valence electron density $n(\mathbf{r})$ from the previous ionic relaxation to correct the total free energy by E_{dipc} in Eq. (6), where the dipole potential Φ is determined directly from the plane-averaged electrostatic potential of the PbTe/CdTe slab.

In general this procedure has to be done self-consistently, i.e., after the correction of the electrostatic potential and the total free energy, the electron density $n(\mathbf{r})$ has to be recalculated. This leads to a new electrostatic potential, which has to be used to update the energy correction term and the compensating field and so on. However, in practice, we perform just the first iteration step, which can be considered as a first-order correction. This results in a uncertainty of about 0.04 J/m^2 for the interface energies of the polar slabs considered.

D. Wulff construction

As mentioned above, the equilibrium crystal shape (ECS) of PbTe nanocrystallites embedded in a CdTe matrix should depend mainly on the interface energies. The anisotropy of $E_{\mathrm{free}}^{\mathrm{inter}}(hkl)$ with respect to the interface orientation $[hkl]$ leads to ECSs different from a sphere; the latter corresponds to the case of perfectly isotropic interface energies. Our calculation of the ECS is based on the Wulff theorem,[33] which states that the ECS is determined by the minimal interface energy F of the crystallite under the constraint of a fixed volume V and a fixed number of Pb atoms. The PbTe quantum dot is assumed to be at least mesoscopic-or nanometer-sized in such way that the energy terms corresponding to the edges and vertices can be neglected. The interface energy with respect to the total interface area $A=A(V)$ is given by

$$F = \oint_{A(V)} E_{\mathrm{free}}^{\mathrm{inter}}(hkl) d\mathbf{A}, \tag{7}$$

where the interface element $d\mathbf{A}=\mathbf{n}\, dA$ is parallel to the normal $\mathbf{n}$ of the facet (hkl).

III. RESULTS AND DISCUSSION

A. Relativistic effects

One expects strong relativistic effects due to the occurrence of heavy elements in the telluride heterostructures under consideration. For electronic properties such as band gaps, effective masses, and similar quantities, that is certainly the case. However, for structural properties the neglect of relativistic and spin effects is a reliable approximation. Not only for tellurides but also for other compounds such as group-III nitrides, the inclusion of spin-orbit effects does not have a significant influence on the structure.[45] As shown in Table I, spin-polarization and spin-orbit effects have only a marginal influence on the values of the equilibrium lattice

TABLE II. Atomic displacements (in Å) at the interfaces with respect to the ideal starting coordinates for the first two interface layers (1) and (2). In the nonpolar case displacements in normal [110] direction (upper line) and parallel to the cubic axis [001] (second line) are listed. In the case of polar interfaces only normal displacements are shown. The interface termination is derived from the ZB structure. In all other directions displacements are not observed.

Interface	$Te(1)_{PbTe}$	$Te(2)_{PbTe}$	$Pb(1)_{PbTe}$	$Pb(2)_{PbTe}$	$Te(1)_{CdTe}$	$Te(2)_{CdTe}$	$Cd(1)_{CdTe}$	$Cd(2)_{CdTe}$
(110)	∓0.15	∓0.12	∓0.24	∓0.02	∓0.09	±0.08	±0.17	∓0.04
(110)	0.25	0.30	0.38	0.35	−0.16	−0.27	−0.24	−0.27
$(100)_{Te\text{-}term.}$	±0.05	±0.00	±0.16	±0.23	∓0.03	∓0.05	∓0.10	∓0.07
$(100)_{Cd\text{-}term.}$	±0.05	∓0.18	∓0.41	∓0.24	±0.29	±0.25	±0.30	±0.29
$(111)_{Te\text{-}term.}$	∓0.02	∓0.04	±0.22	±0.16	∓0.05	∓0.05	∓0.07	∓0.06
$(111)_{Cd\text{-}term.}$	±0.06	∓0.09	∓0.32	∓0.26	±0.20	±0.15	±0.24	±0.17

constants. The excellent agreement with experimental values (apart from the well-known LDA overbinding effect) demonstrates that the LDA exchange-correlation functional is accurate enough to allow investigations of the atomic displacements at CdTe/PbTe interfaces. This observation may be traced back to the electron distributions in the two bulk materials, which have spin-paired electrons and no magnetic ordering. For ZB-CdTe each of the four bonds in the unit cell is occupied with two paired electrons. In RS-PbTe the bond ionicity is so large that Pb^{a+} (Te^{a-}) ions appear, whose outermost electron shells are nearly empty (filled). Here a stands for a number close to 2.

B. Atomic displacements

To obtain the atomic displacements of different interfaces shown in Table II, we allowed ionic relaxation until the x, y, and z components of the interatomic forces are less than 0.02 eV/Å. Figure 3 shows schematic ball-and-stick representations of the relaxed interface geometries.

The combination of the polar ZB-CdTe (100) and (111) surfaces with the corresponding RS-PbTe surfaces gives rise to interfaces with different terminations of the ZB crystal. These A and B interfaces are completely different with respect to extent (averaged distance of the outermost atomic planes of the two crystals) and bonding behavior, as a consequence of the construction principle discussed in Sec. II B. At (100)/(111) interfaces with a Cd termination of the ZB crystal we find a nominal interface extent of $(a_0/4)/(\sqrt{3}a_0/12)$, whereas the extent at Te-terminated interfaces is found to be $(a_0/2)/(\sqrt{3}a_0/4)$, in good agreement with recent HRTEM investigations.[5] In both cases only displacements parallel to the interface normal occur. The main effect is some kind of rumpling, known from the free PbTe(100) surface.[14] At Cd-terminated interfaces this effect is significant larger than at Te-terminated interfaces, where we find a nearly bulklike geometry. One possible reason for that is the different interface separation. Overall we state that both (100) and (111) interfaces show a very similar behavior.

At the nonpolar (110) interface the rumpling effect results in a weak splitting of the electrostatic neutral and stochiometric PbTe(110) planes into bilayers. The effect vanishes in the slab center and increases toward the interfaces. The split bilayers change the polarity in an oscillating way. But the most prominent effect at this kind of interfaces is an offset of 0.38 Å in the [001] direction (parallel to the interface) between the PbTe and CdTe crystals, which may be interpreted as the result of two tendencies. First of all the $Cd(1)_{CdTe}$ atoms try to occupy a fourfold-coordinated site and second

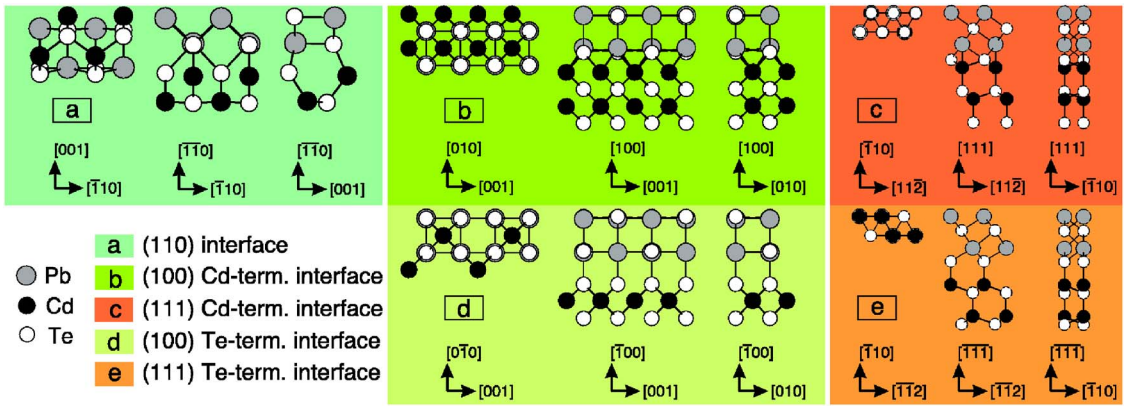

FIG. 3. (Color online) Schematic representation of the atomic arrangements at the relaxed PbTe/CdTe interfaces [left panel, (110) face; middle panel, (100) face; and right panel, (111) face]. In the case of the polar (100) and (111) faces the upper panel shows the Cd-terminated and the lower panel the Te-terminated interfaces. The atoms are represented by open (Te), filled (Cd), and shaded (Pb) circles.

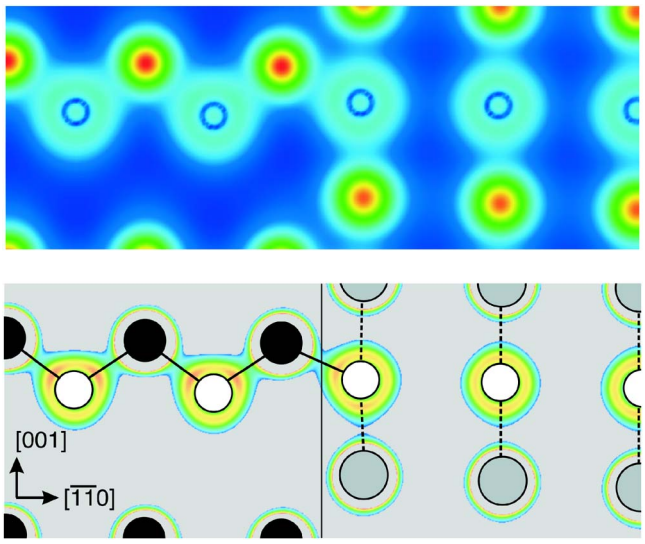

FIG. 4. (Color online) Valence electron density (in arbitrary units) in a (1$\bar{1}$0) plane around the (110) interface (indicated as straight line). The color scale varies from very low densities [blue (light gray)] to very high densities [red (dark gray)]. The upper panel shows the complete valence electron density, while the lower panel shows the restricted valence electron density, where the gray fields correspond to regions with almost zero (or rather high) densities. The atoms are represented by open (Te), filled (Cd), and shaded (Pb) circles. Partially covalent bonds are shown by solid lines, while mainly ionic bonds are indicated by dashed lines.

there are repulsive forces between the $Pb(1)_{PbTe}$ and $Te(1)_{CdTe}$ ions.

To verify this idea, we have plotted the valence electron density $n(\mathbf{r})$ in Fig. 4 (top panel). Due to the treatment of the Cd 4*d* and Pb 5*d* electrons as valence electrons we find very high densities localized at the Cd and Pb ion positions. To enhance the resolution we have restricted the density to values between 0.26 and 0.6 $Å^{-3}$. Therefore the gray regions in Figs. 4 (lower panel) and Fig. 5 correspond to regions with very low (interatomic regions) or very high (regions around the ions) densities. At the (110) interface we find an enhanced valence charge density between the $Cd(1)_{CdTe}$ and the $Te(1)_{CdTe}$ atoms, which gives strong evidence for a partially covalent bond across the interface. The tendency for the formation of such a Cd-Te bond can be understood as a continuation of the zinc-blende structure into the interface region. The 3/4 electron from the Cd sp^3 hybrid may contribute to fill the valence level of the Te atom, which is missing 1/3 electron at the free (110) surface. The bond picture is in good agreement with the obtained interface geometry, where the $Cd(1)_{CdTe}$ is in a fourfold-coordinated site. On the other hand the interaction between the $Pb(1)_{PbTe}$ and $Te(1)_{CdTe}$ atoms is dominated by repulsive electrostatic forces resulting in the small lateral offset between the PbTe and CdTe slabs.

A very similar behavior can be observed at the Cd-terminated (111) interface, where a partially covalent bond between the $Cd(1)_{CdTe}$ and the $Te(1)_{PbTe}$ is formed across the interface; or better to say in the interface region, because in practice it is not possible to define an exact interface layer by construction, i.e., it is not possible to determine to which slab the Te interface layer belongs. Therefore, after atomic relaxation, it is more convenient to refer to an extended interface region than to a sharp interface. Keeping this in mind at the Te-terminated interface a very similar bonding structure is observed. Again a partially covalent bond between the $Cd(1)_{CdTe}$ and the $Te(1)_{CdTe}$ is found. In the same sense as for the (110) interface this effect can be understood as a continuation of the zinc-blende structure into the interface region. In contrast to the nonpolar (110) interface, here the electrostatic forces between the $Pb(1)_{TbTe}$ and $Te(1)_{CdTe}$ ions are parallel to the interface normal. Therefore no displacements parallel to the interface occur.

At the (100) interfaces, we found no evidence for a partially covalent bond inside the interface regions. The bonding between both materials is dominated by electrostatic interactions. This is probably related to the very stable structure of the free RS (100) surface, which has only one missing neighbor per atom.

For subsequent comparisons of our results the values of the displacements at the considered interfaces are listed in Table II. The signs of the displacements parallel to the interface normal depend on the stacking order of the PbTe and CdTe slabs along the interface normal. The upper plus and minus signs correspond to the stacking order PbTe/CdTe and the lower signs to the stacking order CdTe/PbTe.

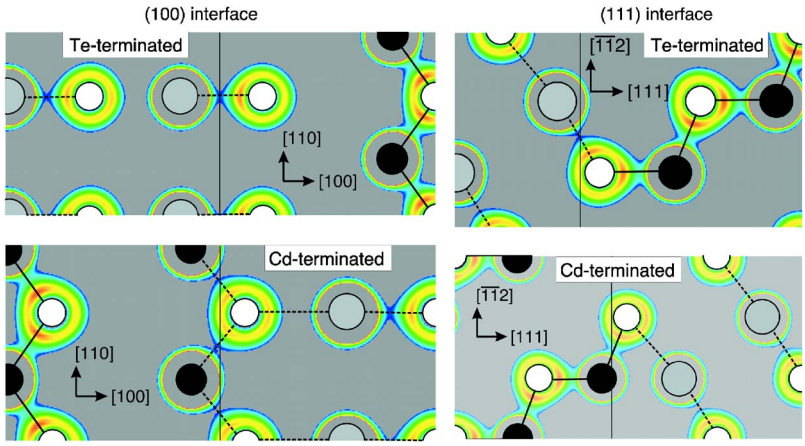

FIG. 5. (Color online) Restricted valence electron density (in arbitrary units): right, in a (1$\bar{1}$0) plane around the (111) interface (indicated as straight line); and left, in a (001) plane around the (100) interface (indicated as straight line). The upper panel shows the Te-terminated and the lower panel the Cd-terminated interfaces. The color scale varies from very low densities [blue (light gray)] to very high densities [red (dark gray)]. The gray fields correspond to regions with almost zero (or rather high) densities. The atoms are represented by open (Te), filled (Cd), and shaded (Pb) circles. Partially covalent bonds are shown by solid lines, while mainly ionic bonds are indicated by dashed lines.

TABLE III. Average interface energies (in J/m^2) for PbTe/CdTe interfaces calculated within the DFT LDA according to Eq. (5) and with the dipole correction of Eq. (6).

Face	(110)	(100)	(111)
LDA	0.20	0.70	0.35
LDA+correction	0.20	0.23	0.19

C. Interface energies and consequences

Once the structural relaxation is performed, the interface energetics can be computed by means of Eqs. (5) and (6). The average interface energies per area A, $\gamma(hkl)=E_{\text{free}}^{\text{inter}}(hkl)/A$, are listed in Table III for three orientations.

The energies of the polar interfaces without the correction term of Eq. (6) are strongly overestimated due to the artificial dipole potential Φ introduced within the supercell approximation. According to the dipole-corrected DFT LDA energies in Table III, the (110) and (100) interfaces, respectively, are the least stable from the energetic point of view. However, the energy differences are smaller than the accuracy of our calculations, which is about 0.04 J/m^2. All three interface energies are roughly close to their average value 0.2 J/m^2. But in contrast to the corresponding free surfaces there is no clear physical trend for the average interface energies in Table III. In agreement with the surface polarity and the number of dangling bonds the surface energies show a relatively clear ordering $\gamma(110)<\gamma(111)<\gamma(100)$ for zinc blende and $\gamma(100)<\gamma(110)<\gamma(111)$ for rocksalt. The same order of surface energies versus orientations was predicted by other authors for ZB-InAs and RS-NaCl.[43,47] The difference in energy ordering of the two sequences does not suggest a unique picture for RS and ZB interfaces, but it confirms the weak variation with the orientation of the corrected averaged energies in Table III.

We use the obtained interface energies to predict the ECS of embedded PbTe nanocrystallites by means of a Wulff construction. The obtained ECSs are presented in Fig. 6 (top panel). They demonstrate a remarkable sensitivity of the shape with respect to tiny variations of the interface energies. Concerning the three interface orientations [110], [100], and [111], we always find a rhombocubo-octahedral ECS. Only the relative ratios of the areas of the {110}, {100}, and {110} facets vary with the absolute values of the interface energies. In any case, Fig. 6 clearly indicates that the three interfaces {110}, {100}, and {111} are thermodynamically stable. The resulting shape may be interpreted as a consequence of the cubic symmetry of both nanocrystal and host material. It may be constructed by a regular octahedron with {111} interfaces truncated at each apex by {100} planes perpendicular to the cube axes but at similar distances from the octahedron centers. In addition to this, the 12 edges of the octahedron are replaced by {110} facets.

The (110) projections of the ECSs shown in Fig. 6 (lower panel) are compared to a HRTEM image of a real PbTe quantum dot embedded in CdTe matrix of Ref. 4. The projections indicate the best agreement for a Wulff construction

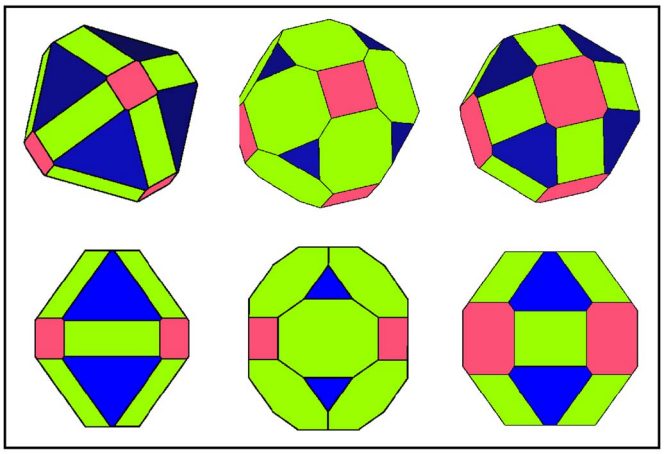

FIG. 6. (Color online) The upper panel shows equilibrium crystal shapes of PbTe embedded in CdTe matrix (not shown). The green facets represent {110}, the red facets {100}, and the blue facets {111} faces. The ECS at the left is constructed using the values of Table III, for the ECS at the middle we have changed the (111) interface energy to 0.22 J/m^2 (within the estimated error bar), and the ECS at the right is constructed using equal interface energies of 0.2 J/m^2. In the lower panel a projection along the [110] zone axis, with the abscissa along $[1\bar{1}0]$ and the ordinate along [001], is shown.

with interface energies of 0.20, 0.23, and 0.22 J/m^2 for the {110}, {100}, and {111} facets, respectively.

The ECR constructed with the dipole-corrected values from Table III seems to have poorer agreement with the experimental observations of Heiss and co-workers.[4] However, the shape of the experimentally observed dots varies slightly with the size, confirming the small variation of the interface energies with respect to the orientation. On the other hand, there are at least two limiting factors of our theoretical description. First, the ECS given by the Wulff construction is very sensitive to the calculated interface energies and the latter have a relatively large uncertainty in this case. By varying the interface energies in the range of the energy error bar, one could in principle obtain ECSs, which are very similar to the nanocrystallite shown in Ref. 4. Second, the energy contribution due to the edges and vertices can have a considerable influence on the stability of small nanocrystallites. For more accurate predictions of the ECS of small PbTe quantum dots, one has to perform explicit *ab initio* calculations for PbTe quantum dots embedded in a CdTe matrix, or at least, to model the system with capped nanocrystallites as suggested in Ref. 48.

IV. SUMMARY AND CONCLUSIONS

We investigated structural and energetic properties of PbTe/CdTe interfaces, which consist of two different cubic crystal structures with partially ionic bonds. An *ab initio* total-energy method was applied to derive the equilibrium atomic positions at the interfaces and to compute the interface energies. The results were combined with a thermodynamic method to construct the equilibrium shape of a PbTe

nanocrystal embedded in a CdTe matrix. We reported a method to calculate the interface energies of polar interfaces within the repeated-slab approximation with an accuracy of about $0.04\ \mathrm{J/m^2}$. Our results predict that the PbTe/CdTe(111) interface is the most energetically favorable interface, whereas the (100) and (110) interfaces are the least stable ones. The variation of the interface energies with respect to the orientation is small. Based on these interface energies and on the Wulff construction, we proposed an equilibrium crystal shape for a PbTe quantum dot embedded in CdTe host matrix. The shape represents a rhombocuboctahedron with 26 interface facets. The relative size of the facet areas for different orientations depends sensitively on the actual relative values of the interface energies. Orthogonal projections of the shape exhibit strong similarities with HRTEM images of PbTe quantum dots in a CdTe matrix.

ACKNOWLEDGMENTS

We acknowledge valuable discussions with F. Schäffler (Linz) and Heiko Groiss (Linz). The work was financially supported through the Fonds zur Förderung der Wissenschaftlichen Forschung (Austria) in the framework of SFB25, Nanostrukturen für Infrarot-Photonik (IR-ON), and the EU NANOQUANTA network of excellence (Grant No. NMP4-CT-2004-500198). Grants of computer time from the Höchstleistungsrechenzentrum Stuttgart are gratefully acknowledged.

*Electronic address: roman@ifto.physik.uni-jena.de

[1] R. C. Ashoori, Nature (London) **379**, 413 (1996).
[2] G. Schedelbeck, W. Wegscheider, M. Bichler, and G. Abstreiter, Science **278**, 1792 (1997).
[3] M. Bayer, P. Hawrylak, K. Hinzer, S. Fafard, M. Korkusinski, Z. R. Wasilewski, O. Stern, and A. Forchel, Science **291**, 451 (2001).
[4] W. Heiss, H. Groiss, E. Kaufmann, M. Böberl, G. Springholz, F. Schäffler, K. Koike, H. Harada, and M. Yano, Appl. Phys. Lett. **88**, 192109 (2006).
[5] R. Leitsmann, L. E. Ramos, F. Bechstedt, H. Groiss, F. Schäffler, W. Heiss, K. Koike, H. Harada, and M. Yano (unpublished).
[6] J. Stangl, V. Holy, G. Bauer, and C. B. Murray, Rev. Mod. Phys. **76**, 725 (2004).
[7] T. Takagi, H. Takaoka, and Y. Kuriyama, Thin Solid Films **126**, 149 (1985).
[8] S. D. Darchuk, S. V. Plyatsko, F. F. Sizov, M. V. Apatskaya, and O. A. Yakubtsov, Optoelectron. Poluprovodn. Tekh. **16**, 84 (1989).
[9] S. Movchan, F. Sizov, and V. Tetyorkin, Semicond. Phys., Quantum Electron. Optoelectron. **2**, 84 (1999).
[10] K. Koike, T. Hounden, I. Makabe, F. P. Yan, and M. Yano, J. Cryst. Growth **257**, 212 (2003).
[11] E. V. Alonso, K. A. Baragiola, J. Ferron, M. M. Jakas, and A. Oliva-Plono, Phys. Rev. B **22**, 80 (1980).
[12] C. B. Duke, A. Paton, W. K. Ford, A. Kahn, and G. Scott, Phys. Rev. B **24**, 3310 (1981).
[13] S. Gundel, A. Fleszar, W. Faschinger, and W. Hanke, Phys. Rev. B **59**, 15261 (1999).
[14] A. A. Lazarides, C. B. Duke, A. Paton, and A. Kahn, Phys. Rev. B **52**, 14895 (1995).
[15] A. Satta and S. de Gironcoli, Phys. Rev. B **63**, 033302 (2001).
[16] F. Bechstedt, *Principles of Surface Physics* (Springer-Verlag, Berlin, 2003).
[17] D. Schiferl, Phys. Rev. B **10**, 3316 (1974).
[18] C. R. A. Catlow and A. M. Stoneham, J. Phys. C **16**, 4321 (1983).
[19] M. Schlüter, G. Martinez, and M. L. Cohen, Phys. Rev. B **11**, 3808 (1975).
[20] J. P. Walter and M. L. Cohen, Phys. Rev. B **4**, 1877 (1971).
[21] S.-H. Wei and A. Zunger, Phys. Rev. B **55**, 13605 (1997).
[22] E. A. Albanesi, E. L. P. y Blanca, and A. G. Petukhov, Comput. Mater. Sci. **32**, 85 (2005).
[23] E. A. Albanesi, C. M. I. Okoye, C. O. Rodriguez, E. L. P. y Blanca, and A. G. Petukhov, Phys. Rev. B **61**, 16589 (2000).
[24] M. Cardona, N. E. Christensen, and G. Fasol, Phys. Rev. B **38**, 1806 (1988).
[25] Y. Al-Douri, R. Khenata, Z. Chelahi-Chikr, M. Driz, and H. Aourag, J. Appl. Phys. **94**, 4502 (2003).
[26] A. A. Stekolnikov and F. Bechstedt, Phys. Rev. B **72**, 125326 (2005).
[27] M. C. Payne, M. P. Teter, D. C. Allan, T. A. Arias, and J. D. Joannopoulos, Rev. Mod. Phys. **64**, 1045 (1992).
[28] L. Quiroga, A. Camacho, L. Brey, and C. Tejedor, Phys. Rev. B **40**, 3955 (1989).
[29] W. R. L. Lambrecht, B. Segall, and O. K. Andersen, Phys. Rev. B **41**, 2813 (1990).
[30] C. Raffy, J. Furthmüller, and F. Bechstedt, J. Phys.: Condens. Matter **14**, 12725 (2002).
[31] J. Neugebauer and M. Scheffler, Phys. Rev. B **46**, 16067 (1992).
[32] M. Bockstedte, A. Kley, J. Neugebauer, and M. Scheffler, Comput. Phys. Commun. **107**, 187 (1997).
[33] G. Wulff, Z. Kristallogr. Mineral. **34**, 449 (1901).
[34] C. Herring, Phys. Rev. **82**, 87 (1951).
[35] G. Kresse and J. Furthmüller, Comput. Mater. Sci. **6**, 15 (1996).
[36] G. Kresse and J. Furthmüller, Phys. Rev. B **54**, 11169 (1996).
[37] D. Hobbs, G. Kresse, and J. Hafner, Phys. Rev. B **62**, 11556 (2000).
[38] G. Kresse and D. Joubert, Phys. Rev. B **59**, 1758 (1999).
[39] S.-H. Wei and A. Zunger, Phys. Rev. B **37**, 8958 (1988).
[40] H. J. Monkhorst and J. D. Pack, Phys. Rev. B **13**, 5188 (1976).
[41] N. Chetty and R. M. Martin, Phys. Rev. B **45**, 6074 (1992); **45**, 6089 (1992).
[42] K. Rapcewicz, B. Chen, B. Yakobson, and J. Bernholc, Phys. Rev. B **57**, 7281 (1998).
[43] N. Moll, M. Scheffler, and E. Pehlke, Phys. Rev. B **58**, 4566 (1998).
[44] L. Bengtsson, Phys. Rev. B **59**, 12301 (1999).
[45] L. E. Ramos, L. K. Teles, L. M. R. Scolfaro, J. L. P. Castineira, A. L. Rosa, and J. R. Leite, Phys. Rev. B **63**, 165210 (2001).
[46] M. L. Cohen, Phys. Rev. B **32**, 7988 (1985).
[47] D. Wolf, Phys. Rev. Lett. **68**, 3315 (1992).
[48] L. E. Ramos, J. Furthmüller, and F. Bechstedt, Phys. Rev. B **72**, 045351 (2005).